AIAA JOURNAL
Vol. 37, No. 2, February 1999

Finite Volume Discretization Aspects for Viscous Flows on Mixed Unstructured Grids

Andreas Haselbacher,* James J. McGuirk,† and Gary J. Page‡
Loughborough University, Loughborough, England LE11 3TU, United Kingdom

A solution method for compressible turbulent flows on unstructured grids in two dimensions is described. The method can be used on grids consisting of triangular and/or quadrilateral cells. Control volumes are constructed from dual cells, and the solution variables are stored at the vertices of the grid. Grid-transparent algorithms are developed that do not require knowledge of cell types, leading to simple discretization schemes on mixed grids. The inviscid fluxes are computed from limited high-resolution schemes originally developed for unstructured triangular grids. They are easily applied to quadrilateral or mixed grids and are grid transparent. The discretization of the viscous fluxes is studied in detail. A positive, grid-transparent discretization of Laplace's equation is developed. The existence of tangential derivatives in the viscous terms prevents grid transparency. By neglecting tangential derivatives, an approximate form of the viscous fluxes is developed, which recovers grid transparency. The approximate form is shown to be similar to the thin-shear-layer approximation. Results are obtained for a transonic inviscid flow, a laminar separated flow, and a transonic turbulent flow. Different control-volume constructions and quadrilateral, triangular, and mixed grids are assessed using a grid-refinement study. The approximate form of the viscous fluxes is investigated in detail.

Introduction

STRUCTURED-GRID finite volume methods are routinely used for predictions of high-Reynolds-number flows typically encountered in aerospace applications. However, difficulties with the generation of high-quality grids have prompted the move toward unstructured-grid flow-solution methods. Whereas much work has concentrated on the application of unstructured-grid methods for the solution of the Euler equations, rarely have fundamental discretization issues for viscous flows been investigated. Although the current study is restricted to two dimensions, care has been taken to ensure that the examined algorithms extend to three dimensions in a straightforward manner. The generation of suitable grids is not addressed in this study.

Regarding the discretization of the Euler equations, Aftosmis et al.[1] have shown that median-dual schemes (see, e.g., Refs. 2 and 3) suffer from excessive numerical diffusion on triangulated quadrilateral grids. When computing viscous flows on triangular grids, geometric constraints lead to the use of long and thin triangular cells.[4,5] The resulting grids closely resemble triangulated quadrilateral grids, and numerical diffusion must be presumed to increase. For stretched triangulated quadrilateral grids, the containment dual[6] has been shown to lead to much improved results compared to the median dual (see also Ref. 7). The improvement seems to be because the containment dual reduces the influence of the diagonal edges in the grid. However, instead of reducing the influence of the diagonal edges, such edges can be deleted completely, thus leading to mixed triangular–quadrilateral grids. The superior discretization properties of quadrilateral grids compared to triangular grids were investigated numerically and analytically by Carpentier et al.[8] An analytical study by Baker[9] shows that additional errors can be induced on triangulated quadrilateral grids. The reduced number of edges in quadrilateral grids also leads to reduced CPU times because many operations are carried out by looping over edges.

Based on the evidence described, it seems best to employ layers of quadrilateral cells around solid bodies and cover the rest of the domain with triangular cells of rapidly increasing size for accurate and economic computations of high-Reynolds-number flows. Note that the use of grids with different cell types is not a new idea; it was suggested by Nakahashi and Obayashi[10] and Weatherill[11] about 10 years ago. Mixed grids have, however, received relatively little interest since these pioneering efforts. This could be due to concerns voiced in the literature that the existence of different cell types complicates the solution method.[12] Recent examples of the use of mixed grids are by Mavriplis and Venkatakrishnan,[13] Coirier and Jorgenson,[14] and Khawaja et al.[15]

The discretization of the viscous terms is usually investigated by studying Laplace's equation, to which the viscous terms in the Navier–Stokes equations reduce for incompressible flow and constant viscosity. The maximum principle associated with Laplace's equation leads to the requirement that the coefficients arising from the discretization be positive. Barth[16] has shown that a Galerkin finite element discretization of the viscous terms on triangular grids results in positive coefficients on Delaunay grids only. Although this result is of theoretical interest, because it demonstrates the close link between positivity and grid quality, it is of relatively little practical value because Delaunay grids are not ideally suited to viscous flows. Coirier[17] carried out a thorough investigation of finite volume discretizations of viscous fluxes on adaptive Cartesian grids. The investigation was motivated by the observation that a calculation of a low-Reynolds-number laminar flow over a backward-facing step diverged due to strongly nonpositive stencils in the reattachment region.

It can be argued that, for high-Reynolds-number flows without flow separation, the influence of poor viscous stencils will be diminished and does not deserve much attention. However, even when separation is avoided, it seems inappropriate from a fundamental modeling viewpoint to have numerous sophisticated inviscid numerical fluxes in comparison to the little-researched viscous numerical fluxes. Also, turbulence models are extremely sensitive to nonpositive coefficients arising from the discretization. Any discretization technique that ensures positivity is, therefore, desirable.

The contribution of the present work is twofold. First, an upwind flow solution method for mixed triangular–quadrilateral grids is presented. For the Euler equations, the algorithm is completely independent of the cell topology. Second, the discretization of the viscous fluxes on general unstructured grids is studied. A positive discretization is developed for Laplace's equation and extended to

Presented as Paper 97-1946 at the AIAA 13th Computational Fluid Dynamics Conference, Snowmass Village, CO, June 29–July 2, 1997; received Aug. 26, 1997; revision received July 15, 1998; accepted for publication Aug. 21, 1998.

*Graduate Student, Department of Aeronautical Engineering; currently Research Scientist, ABB Corporate Research, Ltd., Section T2, 5405 Baden-Dättwil, Switzerland. E-mail: andreas.haselbacher@chcrc.abb.com.
†Professor of Aerodynamics, Department of Aeronautical Engineering.
‡Lecturer, Department of Aeronautical Engineering.

the Navier–Stokes equations. An approximate form of the viscous fluxes is devised that is independent of the cell topology.

Governing Equations

The fluid motion is governed by the Reynolds-averaged Navier–Stokes equations, expressed in integral form for a control volume Ω with boundary $\partial\Omega$ and outward unit normal $\boldsymbol{n}$:

$$\frac{\partial}{\partial t}\int_{\Omega} \boldsymbol{u}\,\mathrm{d}A + \oint_{\partial\Omega} \boldsymbol{f}\cdot\boldsymbol{n}\,\mathrm{d}s = \oint_{\partial\Omega} \boldsymbol{g}\cdot\boldsymbol{n}\,\mathrm{d}s \tag{1}$$

where $\boldsymbol{u}$ represents the state vector of conserved variables and $\boldsymbol{f}$ and $\boldsymbol{g}$ are the corresponding inviscid and viscous flux vectors. In a Cartesian coordinate system with unit vectors $\boldsymbol{i}$ and $\boldsymbol{j}$, the state and flux vectors can be written as

$$\boldsymbol{u} = \begin{Bmatrix} \rho \\ \rho u \\ \rho v \\ \rho E \end{Bmatrix}, \qquad \boldsymbol{f} = \begin{Bmatrix} \rho u \\ \rho u^2 + p \\ \rho uv \\ \rho uH \end{Bmatrix} \boldsymbol{i} + \begin{Bmatrix} \rho v \\ \rho uv \\ \rho v^2 + p \\ \rho vH \end{Bmatrix} \boldsymbol{j}$$

$$\boldsymbol{g} = \begin{Bmatrix} 0 \\ \tau_{xx} \\ \tau_{yx} \\ \tau_{xx}u + \tau_{xy}v - q_x \end{Bmatrix} \boldsymbol{i} + \begin{Bmatrix} 0 \\ \tau_{xy} \\ \tau_{yy} \\ \tau_{yx}u + \tau_{yy}v - q_y \end{Bmatrix} \boldsymbol{j}$$

where ρ is the density, $\boldsymbol{v} = \{u, v\}^t$ is the velocity vector, p is the pressure, and H is the total enthalpy. The ideal gas law is assumed to apply, i.e.,

$$p = R\rho T = (\gamma - 1)\rho\left(E - \tfrac{1}{2}\|\boldsymbol{v}\|^2\right) \tag{2}$$

where R is the gas constant, T is the temperature, and γ is the ratio of specific heats, taken as 1.4.

The effects of turbulence are modeled through the eddy-viscosity hypothesis. The stress tensor is then given by

$$\boldsymbol{\tau} = 2(\mu + \mu_t)\boldsymbol{S} - \tfrac{2}{3}(\mu + \mu_t)\nabla\cdot\boldsymbol{v}\boldsymbol{I} - \tfrac{2}{3}\mu_t k\boldsymbol{I} \tag{3}$$

where μ is the dynamic viscosity, μ_t is the eddy viscosity, $\boldsymbol{I}$ is the identity tensor, k is the turbulence kinetic energy, and $\boldsymbol{S}$ is the strain tensor.

The heat flux vector is given by Fourier's law:

$$\boldsymbol{q} = -(\kappa + \kappa_t)\nabla T = -\frac{\gamma R}{\gamma - 1}\left(\frac{\mu}{Pr} + \frac{\mu_t}{Pr_t}\right)\nabla T \tag{4}$$

where κ is the coefficient of heat conduction and κ_t is its turbulent transport equivalent. The laminar and turbulent Prandtl numbers are taken to be 0.72 and 0.9, respectively. The variation of dynamic viscosity with temperature is given by Sutherland's law.

At present, the one-equation turbulence model of Spalart and Allmaras[18] is employed.

Solution Algorithm

The finite volume method is employed on unstructured grids composed of triangular and/or quadrilateral cells. Because the present focus is on discretization aspects, speed of convergence is not of primary importance. Therefore, a simple explicit four-stage Runge–Kutta scheme with local time stepping is used. An agglomeration multigrid algorithm is under development. More details can be found in Ref. 19.

Control Volume Definition

The control volumes are constructed from dual cells.[3] This approach defines a control volume for each vertex in the grid, at which solution variables are stored, and a face, through which fluxes are computed, for each edge in the grid.

On triangular, quadrilateral, and mixed grids, the control volumes are constructed from the median dual. On triangular grids, the control volumes can also be constructed from the containment dual.[6]

Data Structure

The present flow solver employs an edge-based data structure. As defined by Barth,[16] this consists of storing pointers to the two vertices of each edge and to the two cells sharing that edge. To be practically useful, the edge-based data structure has to be supplemented by a cell-based data structure.

In the present implementation, the information provided by the data structure is stored in three arrays. The first array lists the two vertices of each edge, the second array lists the two cells sharing each edge, and the third array lists the vertices of each cell. The reasons for this choice will become apparent later.

For the sake of discussion, we will refer to algorithms that can be carried out by looping over edges and make use of the three arrays as just defined as edge-based algorithms.

Grid Transparency

The use of mixed grids raises the question of how the existence of different cell types affects the solution method. Whereas it may be unavoidable to treat triangular and quadrilateral cells differently (or separately) during the pre- and postprocessing stages, we regard it as undesirable to treat triangular and quadrilateral cells differently during the flow solution stage. The resulting conditional statements adversely affect program speed and result in untidy code. Therefore, it is sensible to treat the different cell types in the same way wherever possible. The ideal case is a code that does not require any information on the local cell topology; it is independent of the cell type. Such a code is termed grid transparent. In the present project, every effort has been made to ensure that the resulting code is grid transparent.

A recent paper by Peroomian et al.[20] addressed the development of solution methods for different types of grids or mixed grids. They also labeled their method grid transparent because structured, unstructured, and mixed grids can be handled by the same code. The present authors had not been aware of this work when developing the method described here; the use of the same label is a coincidence. An important difference, however, is that the present method is not simply capable of working on triangular, quadrilateral, or mixed grids. The algorithm does not, in fact, see any difference between such grids for a given set of vertices.

Grid-transparent algorithms are not allowed to refer to cell information. All knowledge of cell topology is restricted to the pre- and postprocessing stages. They can, thus, be regarded as a subset of edge-based algorithms because only part of the information provided by the edge-based data structure is used; the second and third data-structure arrays are not required. This has important implications on the stencils obtained on quadrilateral and mixed grids. For a grid-transparent algorithm, the stencil at a given vertex i will primarily consist only of vertices that are linked to vertex i by an edge. This situation is shown in Fig. 1 for a quadrilateral and a mixed grid, where vertices included in the stencil are denoted by $\times$. If the other vertices, i.e., those that belong to a cell at vertex i but are not linked to vertex i by an edge, are to be involved also, they have to be included in a two-step procedure. In contrast, on a triangular grid, all of the vertices of the cells meeting at a vertex are involved in the stencil at that vertex.

The consequence of using grid-transparent schemes on quadrilateral and mixed grids is, therefore, a potential reduction in the extent of the stencil at a given vertex compared to non-grid-transparent schemes. The resulting advantages are increased program speed and suitability for implicit solution methods and parallel implementation. The accompanying disadvantage is reduced accuracy under grid distortion. In other words, it is important to note that grid transparent does not imply grid-quality transparent. Because we do not believe that highly accurate solutions can be obtained at reasonable cost on distorted grids, we acknowledge the disadvantage but do not regard it as too restricting in practice.

The preceding discussion involves two dimensions, where two cells meet at each interior edge. However, the real benefits of grid-transparent algorithms will be felt only on mixed grids in three dimensions. The number of grid cells meeting at an edge in three dimensions is strongly dependent on the cell types. For example, that number is essentially arbitrary for a tetrahedral grid and may

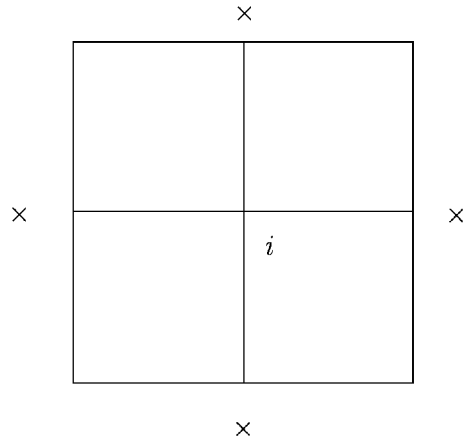

a) Quadrilateral grid

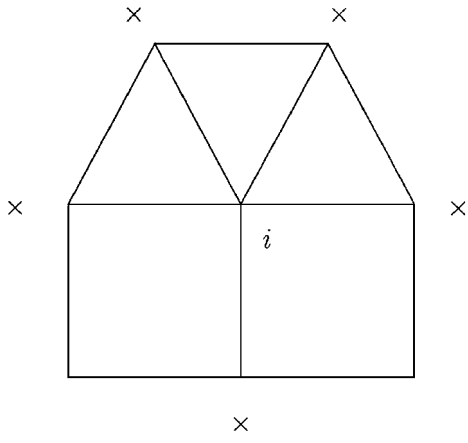

b) Mixed grid

Fig. 1 Grid-transparent stencil, where vertices directly included in stencil are denoted by ×.

vary considerably on mixed grids. It is clear that a substantial simplification will be achieved if one does not have to refer to a large (and variable) number of cells at each edge. A further motivation for the development of grid-transparent methods is the existence of complex polygonal cells on coarse-grid levels when using agglomeration multigrid, where it may not be possible to construct the second and third data-structure arrays described earlier.

The issue of grid transparency will be discussed further as appropriate.

Inviscid Fluxes

Various numerical flux functions, reconstruction methods, and limiter functions have been implemented in the flow solution method. Here, only Roe's flux-differencesplitting,[21] the unweighted linear least-squares reconstruction by Barth,[16] and the limiter function by Venkatakrishnan[22] have been used.

The implementation of the described reconstruction methods and limiter functions can be accomplished by looping over the edges without referring to cell information. They are, therefore, grid transparent.

Viscous Fluxes

Theoretical Considerations

The present investigation of the viscous fluxes was motivated by the desire to obtain a positive, second-order-accurate scheme on arbitrary mixed grids that is compatible with the edge-based data structure and possibly grid transparent. To simplify the analysis, Laplace's equation was studied.

Theoretical studies based on Taylor-series analysis allow an examination of the conditions for local second-order accuracy. The discretized form of Laplace's equation on a general grid can be written as

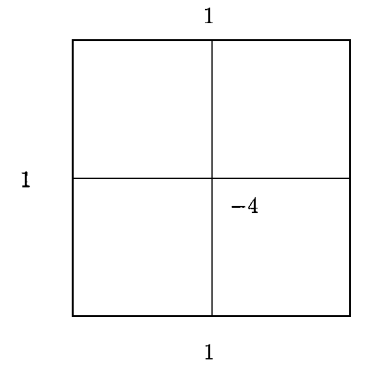

a) Quadrilateral grid

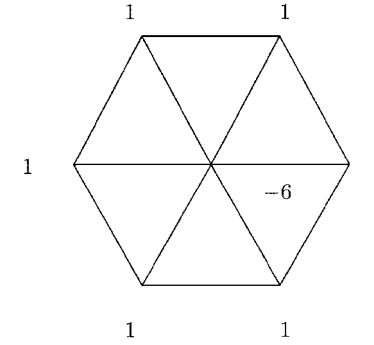

b) Triangular grid

Fig. 2 Classical stencils for Laplacian.

$$(\nabla^2\phi)_0 \approx \sum_{i=1}^{n} \omega_i(\phi_i - \phi_0) = 0 \tag{5}$$

at a grid point 0, where the summation is over n neighboring vertices. The maximum principle associated with Laplace's equation requires the coefficients ω_i to be positive.

The conditions for second-order accuracy can be written as nine equations involving the coefficients ω_i and the coordinate differences over the stencil.[17,23] From these equations, it is easy to show that there is a basic incompatibility between accuracy and positivity of the coefficients on general grids. For arbitrary grid geometries, positivity of the coefficients and second-order accuracy cannot be achieved simultaneously. Both accuracy and positivity can be attained only on regular grids. Note that this conclusion is consistent with the work by Barth[16] on the positivity of the Galerkin finite element discretization of Laplace's equation. More details can be found in Refs. 17 and 19.

For Laplace's equation, the scheme should also result in the classical stencils on regular quadrilateral and triangular grids as shown in Fig. 2. This automatically enforces grid transparency. However, devising such a scheme turns out to be more difficult than expected.

Nonpositive Discretization of Laplacian

For example, consider discretizing Laplace's equation by a finite volume method where the gradients at each face are found from a discrete form of the Green–Gauss theorem,

$$\nabla\phi \approx \frac{1}{A_\Omega} \oint_{\partial\Omega} \phi \boldsymbol{n}\, \mathrm{d}s \tag{6}$$

where the path $\partial\Omega$ is given by the union of the two cells meeting at the edge associated with that particular face. This gives the desired stencil on a regular triangular grid but leads to the so-called rotated Laplacian on a regular quadrilateral grid.[17] This is the stencil where the vertices linked to the central vertex have zero weights, whereas the vertices not directly linked to the central vertex have positive weights, giving poor smoothing properties.

Positive Discretization of Laplacian

A positive discretization for Laplace's equation can be constructed by recalling the identity

$$\int_\Omega \nabla^2\phi \, \mathrm{d}A = \oint_{\partial\Omega} \frac{\partial\phi}{\partial n} \, \mathrm{d}s \tag{7}$$

The key difference from the use of the Green–Gauss theorem is that the normal derivative is discretized directly. Equation (7) is approximated as

$$(\nabla^2\phi)_0 \approx \frac{1}{A_\Omega} \sum_{i=1}^{n} \frac{\Delta s_i}{\Delta n_i} (\phi_i - \phi_0) \tag{8}$$

where Δn_i is the length of the edge connecting vertices 0 and i and Δs_i is the length of the associated dual edge. This discretization satisfies grid transparency. Furthermore, comparing Eq. (8) with Eq. (5) shows that the weights are guaranteed to be positive. Accordingly, Eq. (8) is referred to as the positive scheme.

On irregular grids, the Green–Gauss theorem discretization is nonpositive but more accurate than the positive discretization given by Eq. (8). On regular grids, both schemes give positive coefficients and good accuracy. However, the Green–Gauss theorem discretization leads to the rotated Laplacian on regular quadrilateral grids and is not grid transparent. The inclusion of the normal derivative ensures that the positive scheme reduces to the classical stencils on regular triangular and quadrilateral grids and prevents the occurrence of the rotated Laplacian as already mentioned. The positive scheme is also grid transparent, making it the more attractive of the two schemes described.

Extension to Navier–Stokes Equations

The positive scheme cannot be directly extended to the Navier–Stokes equations because the full viscous terms cannot be written in the form

$$\oint_{\partial\Omega} \mu \nabla\phi \cdot \boldsymbol{n} \, \mathrm{d}s \tag{9}$$

where ϕ is u or v. For example, in the x- and y-momentum equations, the viscous terms can be cast as

$$\oint_{\partial\Omega} \mu \nabla u \cdot \boldsymbol{n} \, \mathrm{d}s + \frac{1}{3} \oint_{\partial\Omega} \mu \nabla \cdot \boldsymbol{v} n_x \, \mathrm{d}s - \oint_{\partial\Omega} \mu \nabla v \cdot \boldsymbol{t} \, \mathrm{d}s \tag{10a}$$

$$\oint_{\partial\Omega} \mu \nabla v \cdot \boldsymbol{n} \, \mathrm{d}s + \frac{1}{3} \oint_{\partial\Omega} \mu \nabla \cdot \boldsymbol{v} n_y \, \mathrm{d}s + \oint_{\partial\Omega} \mu \nabla u \cdot \boldsymbol{t} \, \mathrm{d}s \tag{10b}$$

In each equation, the third term vanishes for constant viscosity due to Stokes' theorem, whereas the second term vanishes for incompressible flow. Even for flows where the second and third terms do not exactly vanish, it is assumed that the most important contribution is due to the first term. Some evidence that substantiates this assumption for laminar flows will be presented subsequently.

It should be noted, however, that the third term in Eq. (10a) and, in particular, Eq. (10b) may not be negligible when eddy-viscosity turbulence models are employed. This is because the essentially constant dynamic viscosity is replaced by the sum of the dynamic viscosity and the strongly varying eddy viscosity. The validity of neglecting the third term in Eq. (10b) will be investigated subsequently.

We have explored two routes for discretizing the viscous terms.

Full Viscous Fluxes

The first route includes all of the terms in Eqs. (10a) and (10b). Therefore, it is necessary to reconstruct the x and y derivatives separately. This can be done by noting that

$$\frac{\partial\phi}{\partial x} = \frac{\partial\phi}{\partial n} n_x - \frac{\partial\phi}{\partial s} n_y \tag{11a}$$

$$\frac{\partial\phi}{\partial y} = \frac{\partial\phi}{\partial n} n_y + \frac{\partial\phi}{\partial s} n_x \tag{11b}$$

where n_x and n_y are the components of the outward unit normal at a particular dual edge and $\partial\phi/\partial s = \nabla\phi \cdot \boldsymbol{t}$ is the tangential derivative. The first approach, therefore, employs the earlier described method of computing the normal derivative, whereas the Green–Gauss theorem is used to calculate the tangential derivative. The two are combined according to Eqs. (11a) and (11b) to give the gradients in the x- and y-coordinate directions, which are then used to compute the viscous fluxes.

The use of normal and tangential derivative components has been described previously by Holmes and Connell.[24] The present derivation highlights how this decomposition naturally arises from studying Laplace's equation and the viscous terms in the Navier–Stokes equations.

The use of the Green–Gauss theorem for the approximation of the tangential derivative prevents grid transparency for viscous flows on mixed grids. Also note that the need for the approximation of the tangential derivatives can occasionally introduce small negative weights under adverse grid conditions for vertices that are not directly linked to the central vertex.

Approximate Form of the Viscous Fluxes

The second route resorts to an approximate treatment to enable grid transparency for the viscous fluxes on mixed grids. Neglecting the last term in Eqs. (10a) and (10b) and approximating the second term using Eqs. (11a) and (11b), where the influence of the tangential derivative is assumed to be small, gives

$$\oint_{\partial\Omega} \mu \nabla u \cdot \boldsymbol{n} \, \mathrm{d}s + \frac{1}{3} \oint_{\partial\Omega} \mu \left(\nabla u \cdot \boldsymbol{n} n_x^2 + \nabla v \cdot \boldsymbol{n} n_x n_y \right) \mathrm{d}s \tag{12a}$$

$$\oint_{\partial\Omega} \mu \nabla v \cdot \boldsymbol{n} \, \mathrm{d}s + \frac{1}{3} \oint_{\partial\Omega} \mu \left(\nabla u \cdot \boldsymbol{n} n_x n_y + \nabla v \cdot \boldsymbol{n} n_y^2 \right) \mathrm{d}s \tag{12b}$$

These are easily approximated along each edge and do not require knowledge of the cell topology. Positivity of the coefficients is guaranteed.

An examination of the neglected terms reveals that the approximation can be regarded as a kind of thin-shear-layer approximation in all coordinate directions. Gnoffo[25] presented a systematic derivation of the formulation of the viscous terms in general three-dimensional curvilinear coordinates. Retaining Gnoffo's nomenclature, a thin-layer approximation in the χ-coordinate direction was derived as

$$\tau_{ns} = \mu \left(\frac{\partial v}{\partial \chi} + \frac{1}{3} \frac{\partial U}{\partial \chi} n_s \right) \nabla\chi \cdot \boldsymbol{n} \tag{13}$$

where τ_{ns} is the shear stress acting in the s-coordinate direction on a control-volume face with outward unit normal vector $\boldsymbol{n}$, v is a dummy variable for u or v corresponding to the coordinate direction s, and U is the control volume face normal velocity. Putting $\chi = y$ and $s = x$ gives

$$\tau_{nx} = \mu \left[\frac{\partial u}{\partial y} + \frac{1}{3} \left(\frac{\partial u}{\partial y} n_x + \frac{\partial v}{\partial y} n_y \right) n_x \right] n_y \tag{14}$$

which is the expression to which the integrands in Eq. (12a) effectively reduce for control-volume faces that are approximately aligned with the x-coordinate direction.

For the viscous fluxes in the energy equation, the stresses are approximated using velocity gradients from Eqs. (11a) and (11b), where the tangential derivative component is neglected. The heat flux is easily approximated, being of the form given by Eq. (9).

In an attempt to derive a simplified discretization of the viscous fluxes on mixed grids, Mavriplis and Venkatakrishnan[13] chose to discretize the full viscous terms on tetrahedral cells only and discretized the Laplacian on pyramidal, prismatic, and hexahedral cells. Although this reduces the required computational work, it cannot be regarded as entirely satisfactory. Assuming that hexahedral and prismatic elements are employed near boundaries, their scheme simplifies the viscous terms in viscous regions, whereas the full viscous terms are retained in regions that are likely to be completely or nearly inviscid. In contrast to the method by Mavriplis and Venkatakrishnan, the present approximation does not depend on the cell type. Instead, it relies more on approximations justified from flow conditions; this is believed to be a better approach.

Peroomian et al.[20] compute the viscous fluxes from a limited reconstruction for the higher-order inviscid fluxes. We do not regard

this as suitable because the limiting of extrema may influence the viscous fluxes.

Results

Results are presented for computational investigations that focus on the influence of grid types on solution quality and the influence of the two forms of the viscous fluxes described earlier. As already stated, the solutions shown here have been obtained with the Roe flux-differences splitting scheme, the unweighted linear least-squares reconstruction method, and the Venkatakrishnan limiter function.

Inviscid Flow

To validate the solution algorithm for the Euler equations, the flow over a circular arc bump in a straight channel is computed. The height of the channel, the distance in front of and behind the bump, and the chord of the bump are equal to one length unit. The transonic case is specified by $M_\infty = 0.675$ and a thickness-to-chord ratio of the bump of 10%.

Solutions have been obtained on a 98×34 regular quadrilateral grid and a triangular grid obtained by inserting diagonals from the bottom-left-hand corner to the top-right-hand corner of each cell.

Figure 3 shows the differences in the pressure coefficient on the lower wall obtained on the quadrilateral grid and on the triangular grid with median and containment dual-control volumes. It can be seen that the solutions on the quadrilateral and the triangular grid with containment dual-control volumes are virtually identical, whereas the median dual-control volume solution exhibits more smearing in the region of the shock wave. Thus, the indication is that, on triangulated quadrilateral grids, the containment dual can attain the same accuracy as the corresponding quadrilateral grid solution. However, the solution on the triangular grid is more expensive by a factor of about 50% due to the greater number of edges.

Laminar Flow

To investigate the formulation of the viscous fluxes and the influence of different grid types, the flow around a NACA 0012 airfoil is computed. The flow is specified by $M_\infty = 0.8$, $Re_\infty = 500$, and $\alpha = 10$ deg. At these conditions, a separation bubble extends over more than half of the upper surface. This test case was used in the GAMM (Gesellschaft für Angewandte Mathematik und Mechanik) Workshop on Numerical Simulation of Compressible Navier–Stokes Flows by Bristeau et al.[26]

The present solutions have been obtained on a series of nested curvilinear grids of 33×9, 65×17, 129×33, and 257×65 grid points. These grids are referred to as the base, coarse, medium, and fine grids, respectively. Triangular grids were obtained by inserting diagonal edges into the quadrilateral grids in such a way that the symmetry of the grids was preserved. Mixed grids were generated by leaving a specified number of layers of quadrilateral cells over the airfoil surface and inerting diagonal edges into the remaining quadrilateral cells. The resulting mixed grids cannot take advantage of rapidly expanding triangular cells toward the far field. The number of quadrilateral layers is equal to five on the base grid and is increased on the finer grids such that the position of the interface between quadrilateral and triangular cells remains identical. The medium quadrilateral, triangular, and mixed grids are shown in Fig. 4.

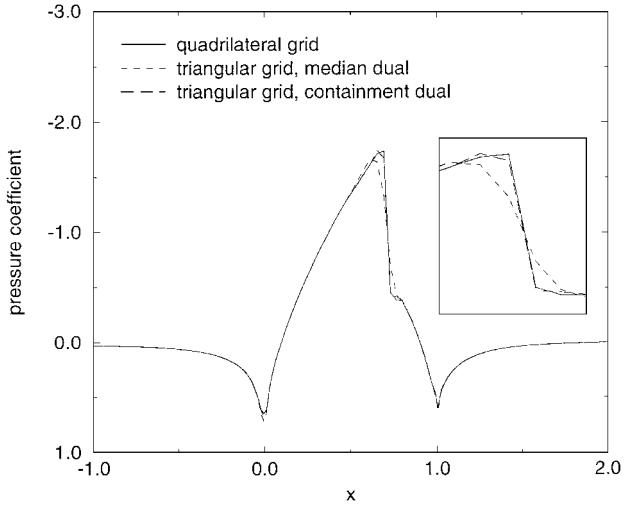

Fig. 3 Pressure coefficient along lower wall for bump flow test case; inset: detail at shock position.

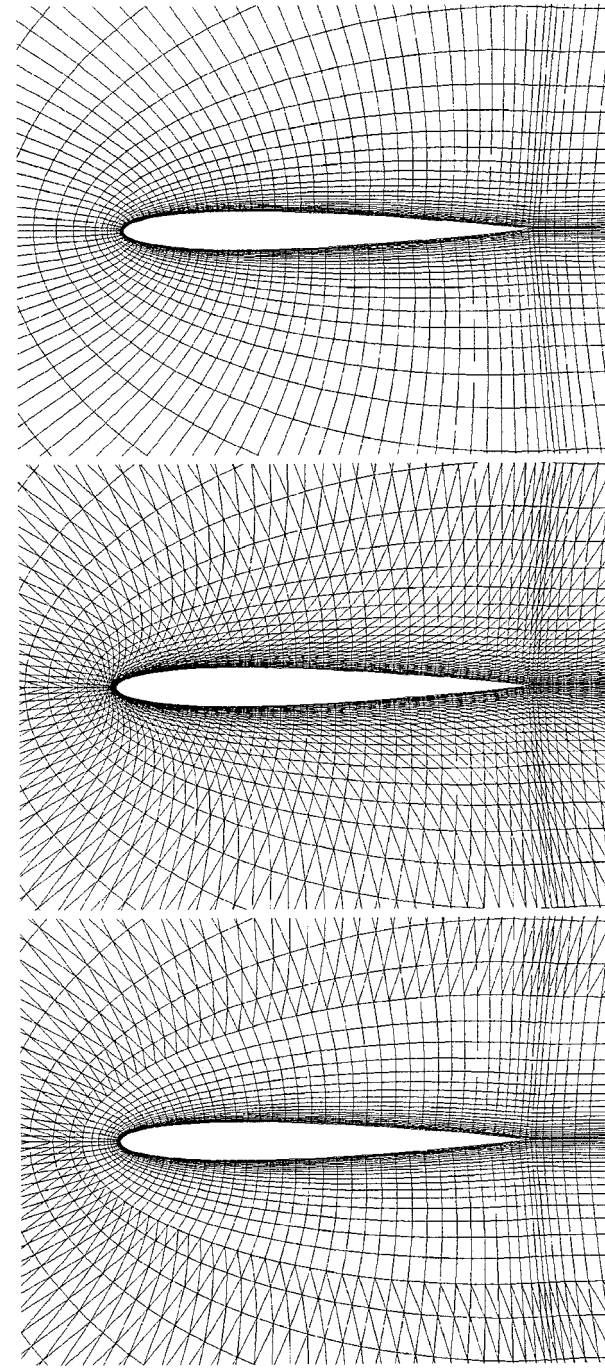

Fig. 4 Quadrilateral, triangular, and mixed-medium grids for NACA 0012 airfoil test case.

To verify the finite volume discretization of the viscous terms given by Eqs. (10a–11b), results obtained with that discretization were compared to those obtained with the well-established Galerkin finite element discretization derived by Barth.[16] It is shown in Ref. 19 that the lift and drag coefficients, as well as separation and reattachment positions, were virtually indistinguishable on each of the four grids, thus confirming the basic validity of the approach described earlier.

A sample of the streamlines on the medium quadrilateral grid is shown in Fig. 5.

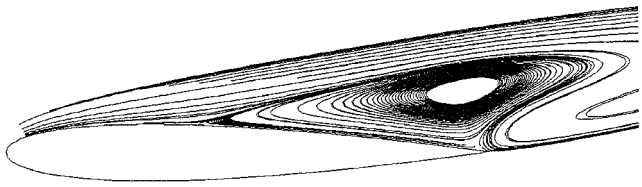

Fig. 5 Streamlines on upper surface for medium quadrilateral grid for NACA 0012 airfoil test case.

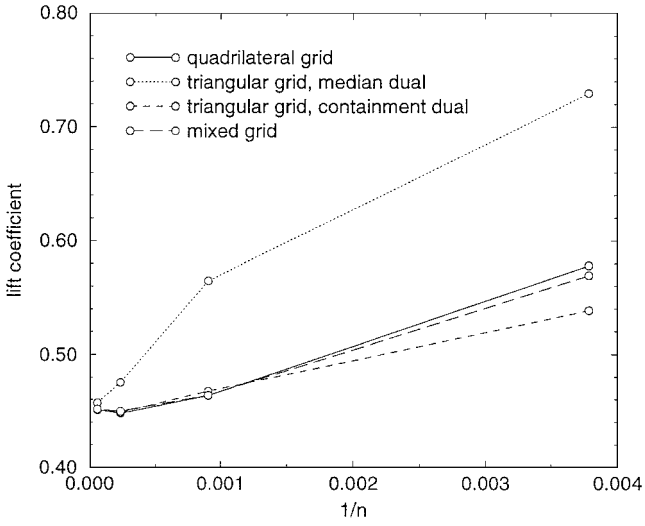

a) Lift coefficient

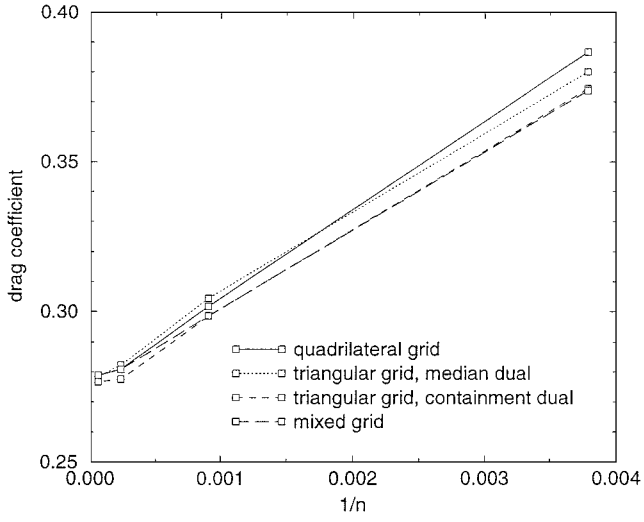

b) Drag coefficient

Fig. 6 Behavior with grid refinement for full viscous terms for NACA 0012 airfoil test case.

Influence of Grid Type

The behavior of the lift and drag coefficients with grid refinement on the quadrilateral, triangular, and mixed grids and the full viscous fluxes is shown in Fig. 6. In this and the following figures showing results of grid refinement studies, abscissas are given by the reciprocal of the number of vertices in the grids. It can be seen from Fig. 6 that the lift coefficient values on the quadrilateral grids, the triangular grids with containment dual-control volumes, and the mixed grids exhibit less variation with grid size than the triangular grids with median dual-control volumes. This indicates that the results on the triangular grids with median dual-control volumes are of a lower level of accuracy. It is interesting to note the nonmonotone behavior of the lift coefficient with grid refinement.

The variation of drag coefficient with grid refinement is quite different in that the four grid types follow approximately the same path. The quadrilateral grid and the triangular grid with containment dual had roughly the same pressure and friction drag components. The triangular grid with median dual-control volumes showed higher pressure and lower friction drag components, partially canceling each other. This seems consistent with earlier observations that the median dual leads to more diffusive results.

The small differences between the lift and drag coefficients on the medium and fine grids indicate that the solutions on those grids are not quite grid independent yet. The solutions may be regarded as nearly grid independent, however, because the differences are much smaller than those on the coarse and medium grids for the same increase in grid density.

Behavior of Approximate Viscous Fluxes

The discretization of the full viscous terms is compared with the approximate form in Fig. 7 for the quadrilateral grids. It can be seen that there is virtually no difference between the two forms. This appears surprising at first because it was shown earlier that the approximate form can be interpreted as a thin-shear-layer approximation. The present flow is of low Reynolds number and is dominated by the large recirculation region. Nevertheless, the approximation seems to be valid. This may also be seen from Fig. 8, where the balance of the terms in Eq. (10a) is plotted along the normal to the upper airfoil surface at $x/c = 0.7$, i.e., in the separation bubble, for the medium quadrilateral grid. The contribution of the Laplacian is clearly the most important. At other chordwise stations, the same result has been observed. The same conclusion applies to the terms

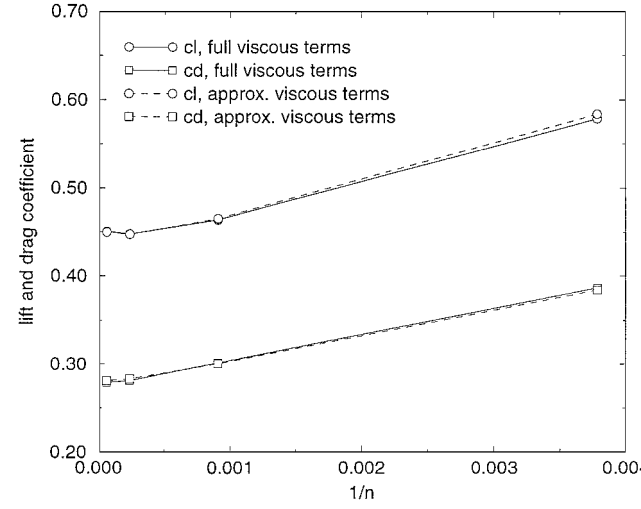

Fig. 7 Lift and drag coefficient behavior with refinement for full and approximate viscous terms on quadrilateral grids for NACA 0012 airfoil test case.

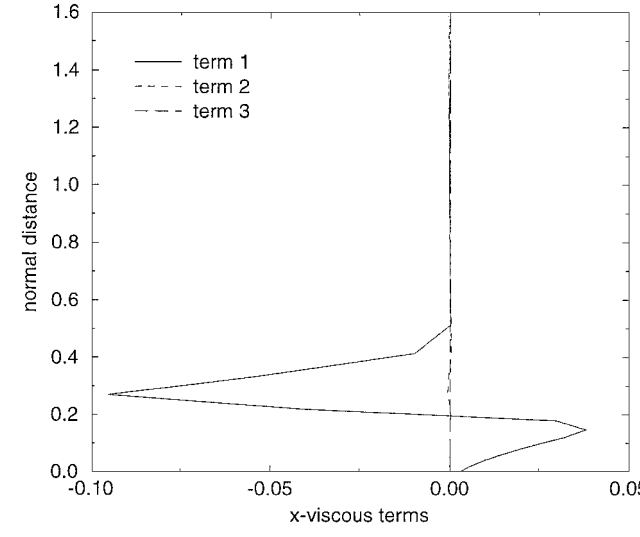

Fig. 8 Relative importance of terms in Eq. (10a) at $x/c = 0.7$ for medium quadrilateral grid for NACA 0012 airfoil test case.

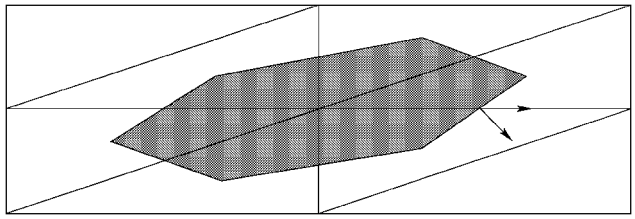

Fig. 9 Median dual-control volume on stretched triangulated quadrilateral grid.

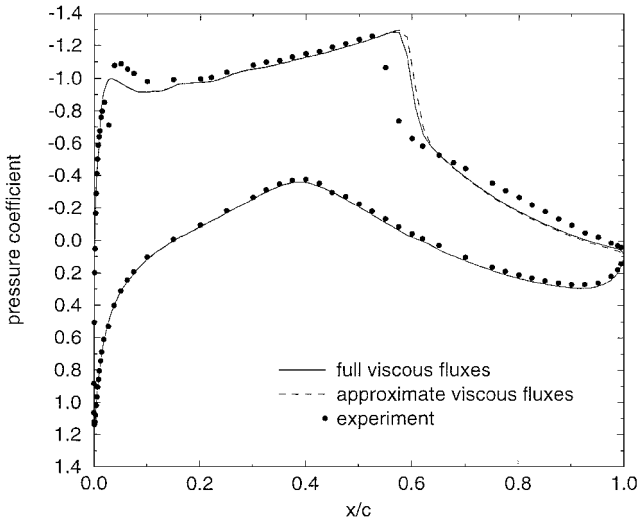

Fig. 10 Comparison of pressure coefficients between full and approximate viscous fluxes on quadrilateral grid for RAE 2822 airfoil test case.

in the y-momentum equation, although the differences are not quite as pronounced, and the magnitude of the terms is reduced.

When employing the approximate form of the viscous fluxes on triangular grids with the median dual, there is relatively poor agreement with the full form. This can be explained by reference to Fig. 9, which shows the median dual-control volume on the type of grid used. The normal derivative is required in the direction of the broken arrow but approximated in the direction of the unbroken arrow. It is easy to see that, even for benign stretching, the normal derivative is not well approximated because the dual edge is not approximately perpendicular to its associated edge. In fact, for the grid shown in Fig. 9, the normal derivative could not be approximated accurately unless another component was used. However, using another component, such as the tangential derivative, reintroduces terms that are not grid transparent.

Because it is not necessary to compute tangential derivatives for the approximate form of the viscous fluxes, savings of up to 20% in CPU time have been achieved when evaluating the viscous fluxes at the first and third steps of the four-step Runge–Kutta scheme. Convergence behavior has been unaffected.

From the results shown in this section, we may conclude that the use of quadrilateral grids, triangular grids with containment dual-control volumes, and mixed grids leads to lower levels of numerical error than the use of median dual-control volumes. Furthermore, the approximate form of the viscous fluxes gives results that are virtually indistinguishable from those obtained with the full form.

Turbulent Flow

The test case involves the solution of the flow around the RAE 2822 airfoil at $M_\infty = 0.754$, $Re_\infty = 6.2 \times 10^6$, and $\alpha = 2.57$ deg. This corresponds to the (corrected) conditions of case 10 in Ref. 27.

The solutions have been obtained on a 257×65 quadrilateral grid with 209 points on the airfoil surface and on a mixed grid with 45 layers of quadrilateral cells. Transition was imposed at $x/c = 0.03$.

Figure 10 shows that there is little difference in terms of pressure coefficient between solutions obtained with the full and approximate

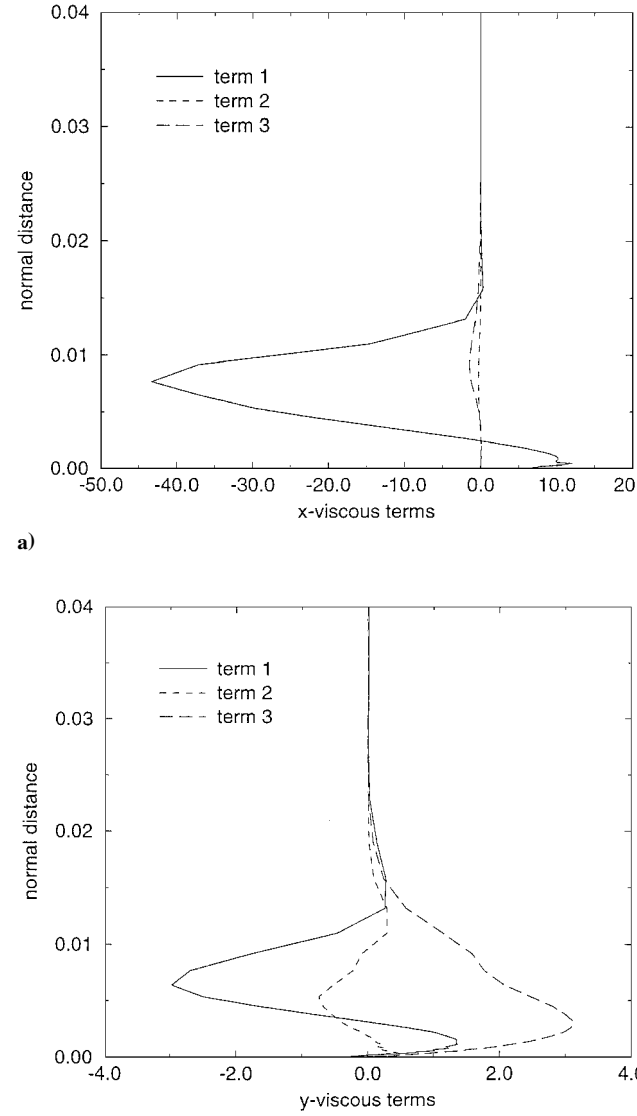

Fig. 11 Relative importance of terms at $x/c = 0.6$ on quadrilateral grid for RAE 2822 airfoil test case: a) in Eq. (10a) and b) in Eq. (10b).

form of the viscous fluxes. Reasonable agreement with experimental values is obtained. Differences between the full and approximate forms are restricted to the shock-wave and separation regions. Values of the lift and drag coefficients were 0.7524 and 0.0275 for the full viscous fluxes and 0.7569 and 0.0276 for the approximate viscous fluxes, respectively. The validity of the approximate form can be assessed from Fig. 11, which shows the importance of the three constituent terms along the normal to the upper airfoil surface at $x/c = 0.6$, i.e., in the interaction region between the shock wave and the boundary layer. It is in this region that we can expect unjustified assumptions in the approximate viscous fluxes to show prominently. The first term in Eq. (10a) clearly dominates the other two, showing that the approximations in the x-momentum equation are justified. In the y-momentum equation, there is no domination of a single term. In particular, as suspected, the third term in Eq. (10b) is not negligible compared to the first term. However, because the magnitude of the terms in Eq. (12b) is roughly an order of magnitude less than those in Eq. (12a), the approximations seem to have little effect.

The comparison of pressure coefficients between the quadrilateral and mixed grids shows little difference, as shown in Fig. 12. The values of the lift and drag coefficient on the mixed grid were 0.7575 and 0.0278. The corresponding experimental values are given by 0.743 and 0.0242. Future work will exploit properly triangulated far-field regions to reduce grid size and, therefore, CPU time.

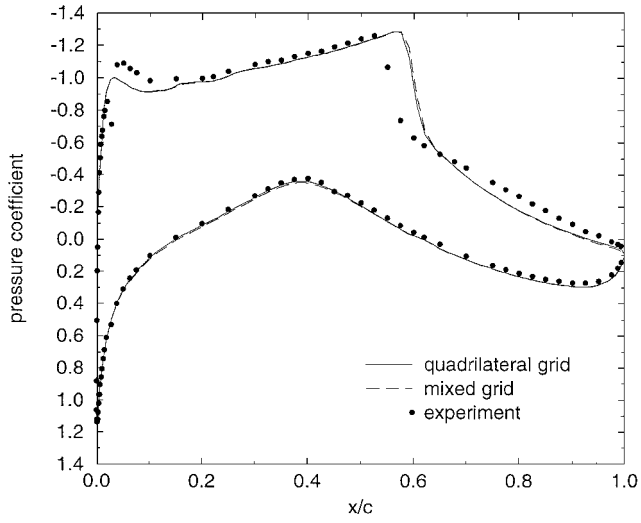

Fig. 12 Comparison of pressure coefficients on quadrilateral and mixed grids for RAE 2822 airfoil test case.

Conclusions

An upwind flow solver for the solution of compressible viscous flows on triangular and/or quadrilateral grids has been described. The concept of grid transparency has been developed, allowing for simple discretization schemes on mixed grids. For the inviscid fluxes, the flow solver is grid transparent. For the viscous fluxes, grid transparency is lost for the full viscous terms. An approximate form of the viscous terms has been derived that is positive and restores grid transparency. The approximate form is similar to the thin-shear-layer approximation.

Numerical results have been presented for a transonic inviscid flow, a laminar flow about an airfoil with large-scale separation, and a turbulent transonic flow about an airfoil. A grid-refinement study has assessed the accuracy of different control constructions and the influence of triangular, quadrilateral, and mixed grids for viscous flow. Median dual-control volumes on triangular grids resulted in higher numerical errors than the other schemes considered.

The approximate form of the viscous fluxes was assessed in detail. For the test cases considered, the results obtained with the approximate forms were practically indistinguishable from those obtained with the full form, while requiring up to 20% less CPU time.

Acknowledgments

The first author is grateful for financial support by the Department of Aeronautical Engineering and through an Overseas Research Student Award (ORS/94026007) by the Committee of Vice-Chancellors and Principals of the Universities of the United Kingdom. The first author would like to acknowledge helpful discussions with William Coirier (CFD Research Corporation) on the discretization of the viscous fluxes on unstructured grids.

References

[1]Aftosmis, M., Gaitonde, D., and Tavares, T. S., "Behavior of Linear Reconstruction Techniques on Unstructured Meshes," *AIAA Journal*, Vol. 22, No. 11, 1995, pp. 2038–2049.

[2]Vijayasundaram, G., "Transonic Flow Simulations Using an Upstream Centered Scheme of Godunov in Finite Elements," *Journal of Computational Physics*, Vol. 63, April 1986, pp. 416–433.

[3]Barth, T. J., and Jespersen, D. C., "The Design and Application of Upwind Schemes on Unstructured Meshes," AIAA Paper 89-0366, Jan. 1989.

[4]Babuška, I., and Aziz, A. K., "On the Angle Condition in the Finite Element Method," *SIAM Journal on Numerical Analysis*, Vol. 13, No. 2, 1976, pp. 214–226.

[5]Rippa, S., "Long and Thin Triangles Can Be Good for Linear Interpolation," *SIAM Journal on Numerical Analysis*, Vol. 29, No. 1, 1992, pp. 257–270.

[6]Barth, T. J., and Linton, S. W., "An Unstructured Mesh Newton Solver for Compressible Turbulent Flows and Its Parallel Implementation," AIAA Paper 95-0221, Jan. 1995.

[7]Kasbarian, C., Leclerq, M.-P., Ravachol, M., and Stoufflet, B., "Improvements of Upwind Formulations on Unstructured Meshes," *Proceedings of the Fourth International Conference on Hyperbolic Problems*, Vieweg, Brunswick, Germany, 1992, pp. 363–368.

[8]Carpentier, R., Glinsky, N., and Larrouturou, B., "Schémas décentrées d'ordre deux operant sur des quadrangles ou des triangles: une comparaison," *Proceedings of the First CNES–ONERA Colloquium*, Office National D'Etudes et de Recherche Aérospatiale, Châtillon, France, 1992, p. 15-1.

[9]Baker, T. J., "Discretization of the Navier–Stokes Equations and Mesh-Induced Errors," *Proceedings of the Fifth International Conference on Numerical Grid Generation in Computational Field Simulation*, Mississippi State Univ., Mississippi State, MS, 1996, pp. 209–218.

[10]Nakahashi, K., and Obayashi, S., "FDM-FEM Zonal Approach for Viscous Flow Computations over Multiple Bodies," AIAA Paper 87-0604, Jan. 1987.

[11]Weatherill, N. P., "Mixed Structured–Unstructured Meshes for Aerodynamic Flow Simulations," *Aeronautical Journal*, Vol. 94, April 1990, pp. 111–123.

[12]Baker, T. J., "Prospects and Expectations for Unstructured Methods," *Surface Modelling, Grid Generation, and Related Issues in Computational Fluid Dynamic (CFD) Solutions*, NASA CP-3291, 1995, pp. 273–287.

[13]Mavriplis, D. J., and Venkatakrishnan, V., "A Unified Multigrid Solver for the Navier–Stokes Equations on Mixed Element Meshes," Inst. for Computer Applications in Science and Engineering, Rept. 95-53, Hampton, VA, July 1995.

[14]Coirier, W. J., and Jorgenson, P. C. E., "A Mixed Volume Grid Approach for the Euler and Navier–Stokes Equations," AIAA Paper 96-0762, Jan. 1996.

[15]Khawaja, A., Kallinderis, Y., and Parthasarathy, V., "Implementation of Adaptive Hybrid Grids for 3-D Turbulent Flows," AIAA Paper 96-0026, Jan. 1996.

[16]Barth, T. J., "Numerical Aspects of Computing High-Reynolds Number Flows on Unstructured Meshes," AIAA Paper 91-0721, Jan. 1991.

[17]Coirier, W. J., "An Adaptively-Refined, Cartesian, Cell-Based Scheme for the Euler and Navier–Stokes Equations," NASA TM-106754, Oct. 1994.

[18]Spalart, P. R., and Allmaras, S. R., "A One-Equation Turbulence Model for Aerodynamic Flows," *La Recherche Aerospatiale*, No. 1, Jan. 1994, pp. 5–21.

[19]Haselbacher, A., "A Grid-Transparent Numerical Method for Compressible Viscous Flows on Mixed Unstructured Grids," Ph.D. Dissertation, Dept. of Aeronautical Engineering, Loughborough Univ., Loughborough, England, UK, Oct. 1999.

[20]Peroomian, O., Chakravarthy, S., and Goldberg, U. C., "A 'Grid-Transparent' Methodology for CFD," AIAA Paper 97-0724, Jan. 1997.

[21]Roe, P. L., "Approximate Riemann Solvers, Parameter Vectors, and Difference Schemes," *Journal of Computational Physics*, Vol. 43, Oct. 1981, pp. 357–372.

[22]Venkatakrishnan, V., "Convergence to Steady-State Solutions of the Euler Equations on Unstructured Grids with Limiters," *Journal of Computational Physics*, Vol. 118, April 1995, pp. 120–130.

[23]Kershaw, D. S., "Differencing of the Diffusion Equation in Lagrangian Hydrodynamic Codes," *Journal of Computational Physics*, Vol. 39, Feb. 1981, pp. 375–395.

[24]Holmes, D. G., and Connell, S. D., "Solution of the Two-Dimensional Navier–Stokes Equations on Unstructured Adaptive Grids," AIAA Paper 89-1932, June 1989.

[25]Gnoffo, P. A., "An Upwind-Biased, Point-Implicit Relaxation Algorithm for Viscous, Compressible Perfect-Gas Flows," NASA TP-2953, Feb. 1990.

[26]Bristeau, M. O., Glowinski, R., Periaux, J., and Viviand, H., *Numerical Simulation of Compressible Navier–Stokes Flows*, Vol. 18, Notes on Numerical Fluid Mechanics, Vieweg, Brunswick, Germany, 1987.

[27]Cook, P. H., McDonald, M. A., and Firmin, C. P., "Aerofoil RAE 2822—Pressure Distributions, and Boundary Layer and Wake Measurements," AR-138, AGARD, May 1979.

J. Kallinderis
Associate Editor